Test-case number 35: Flow rate limitation in open capillary channels (PE)

October 31, 2003

Antje Ohlhoff, ZARM, University of Bremen, 28359 Bremen, Germany
Phone: +49 (0)421 218 4788, Fax: +49 (0)421 218 2521
E-Mail: *ohlhoff@zarm.uni-bremen.de*

Uwe Rosendahl, ZARM, University of Bremen, 28359 Bremen, Germany
Phone: +49 (0)421 218 4314, Fax: +49 (0)421 218 2521
E-Mail: *rosend@zarm.uni-bremen.de*

Michael E. Dreyer, ZARM, University of Bremen, 28359 Bremen, Germany
Phone: +49 (0)421 218 4038, Fax: +49 (0)421 218 2521
E-Mail: *dreyer@zarm.uni-bremen.de*

1 Practical significance and interest of the test case

This test case is concerned with the flow rate limitation of a free surface flow through an open capillary channel consisting of two parallel plates. Due to convective and viscous momentum transport the pressure along the flow path decreases and forces the free surfaces to bend inwards. Since the free surfaces can only withstand a certain difference between the liquid and ambient pressure, the flow rate in the channel is limited. This *maximum* or *critical flow rate* is reached when the flow becomes unstable and the surfaces collapse. At that state the flow characteristic changes from a steady single-phase to an unsteady two-phase flow. Our hypothesis is (see Rosendahl *et al.* , 2003) that the collapse of the surface occurs due to the effect of choking, which is known from compressible gas flows and open channel flows under normal gravity. The characteristic number for this effect is defined by the ratio of the mean liquid velocity and the speed of longitudinal waves in open capillary channels. This number tends towards unity in the case of choking at the smallest cross section in the channel. The aim is to predict the critical velocity and the corresponding maximum flow rate as well as the innermost contour lines of the free surfaces for steady flows.

This study presents quantitative data achieved experimentally under reduced gravity conditions on board the sounding rocket TEXUS-37. During the six minutes of a ballistic flight the volume flux has been increased up to the critical value for which the flow becomes unstable and the liquid surfaces collapse. This paper provides the typical video observations of the steady and unsteady flow as well as the evaluated innermost contour lines of the free surfaces, especially the position of the smallest cross section and the maximum velocity as function of the adjusted volume flux for the steady regime. Also the maximum flow rate is provided. All boundary conditions required for numerical calculations are given. Open capillary channels are used in a number of applications in space liquid management, *e.g.* in heat pipes and in surface tension tanks of satellites. However, in spite of the high number of applications the flow through open capillary channels and the related effect of flow rate limitation are not well understood and rarely discussed in the literature. Besides experimental data from drop tower and sounding rocket experiments provided by Rosendahl *et al.* (2002) and Rosendahl *et al.* (2003), only a few one-dimensional steady numerical model computations performed by Jaekle (1991), Srinivasan (2003) and Rosendahl *et al.* (2003) exist. Admittedly one-dimensional assumptions

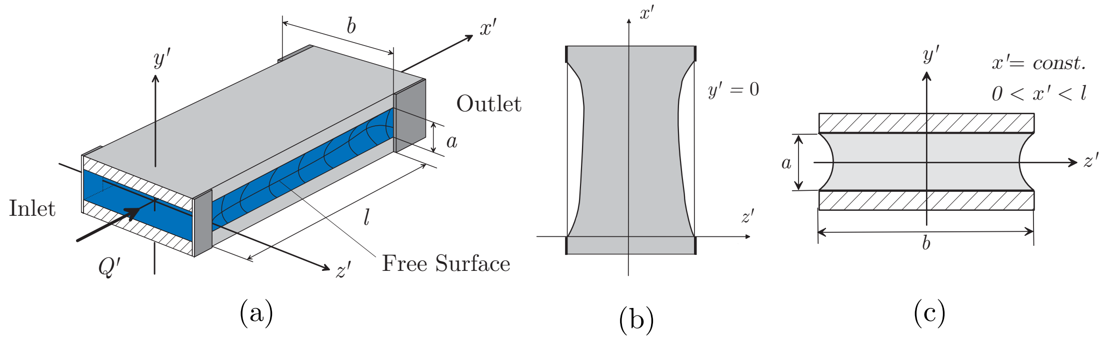

Figure 1: (a) Liquid flow through an open capillary channel consisting of two parallel plates. Due to flow losses the free surfaces along the flow path x' bend inwards. (b) The symmetry plane $y' = 0$ and (c) cross sectional area for $x' =$ const. All values have dimensions.

are not well fulfilled at the inflow and outflow region. For this reason quantitative steady three-dimensional numerical results are desirable as well as time-dependent computations to understand the process of the collapsing flow in detail. The main numerical difficulty is the interaction of a three-dimensional flow with a free surface, which is - above a critical value - additionally an unsteady two-phase flow. As far as our experience goes the determination of the critical volume flux and the quantitative steady contours of the free surfaces is difficult. In the case of viscous dominated flows and time-dependent flows the free surface is no longer pinned at the edges of the channel and moves inwards between the plates. This results in a moving contact line problem. The time-dependent bubble formation at the end of the channel is an interesting challenge too.

2 Definitions and model description

A flow through an open capillary channel as shown in figure 1(a) is considered under low gravity conditions. The channel consists of two parallel plates of distance a, breath b and length l. The flow enters the channel via an inlet with a closed circumference, passes the open section (free surface flow) and leaves it at the outlet (likewise with a closed circumference). The volumetric flow rate Q' is created by external pumps (note that primes are used to denote dimensional variables). The inlet is connected with a liquid reservoir through a nozzle (see 3.1). The reservoir is connected to a compensation tube which applies a known pressure (lower than ambient pressure) to the system. The head losses in the nozzle decrease the pressure even further and determine the boundary condition at the inlet. Due to convective and frictional momentum transport in the open channel the pressure decreases in flow direction and the curvature increases (figure 1(b)). The liquid surfaces are bend inwards at any cross-sectional area of the flow path (figure 1(c)).

We assume an isothermal flow along the channel axis x' characterized by the velocity $\mathbf{u}'(x', y', z') = (u'_{\mathrm{x}}, u'_{\mathrm{y}}, u'_{\mathrm{z}})$ and the liquid pressure $p'(x', y', z')$. The origin of the coordinate system is located in the center of the inlet cross section of the free surface channel. For the analysis all lengths are scaled by half the plates distance $a/2$, except for the cross section A which is scaled by $A_0 = ab$ (all relevant values are listed in table 1). The velocities are scaled by

$$v_0 = \sqrt{\frac{4\sigma}{\rho D_h}}, \tag{1}$$

where σ is the surface tension, ρ the density and $D_h = 2a$ the hydraulic diameter of the channel. This velocity is known from the self-driven inflow of liquid into a capillary parallel plate channel (capillary rise) reported by Dreyer *et al.* (1994). With equation (1) the dimensionless volume flux reads $Q = Q'/(A_0 v_0)$ and the liquid pressure $p = p'/p_0$ with $p_0 = 2\sigma/a$. In the following, all values are dimensionless.

The capillary pressure $p - p_a$ is related to the curvature of the free surface by the normal stress balance (assuming zero normal velocities at the free surface and a passive overlaying gas), generally denoted as GAUSS-LAPLACE equation (Landau & Lifschitz, 1991)

$$p - p_a = -\left(\frac{1}{R_1} + \frac{1}{R_2}\right) = -\kappa. \tag{2}$$

Herein R_1 and R_2 are the principal radii of curvature of the liquid surface, κ is the sum of the curvatures and p_a denotes the ambient pressure.

The scaling yields three dimensionless parameters which are the dimensionless channel length $L = 2l/a$, the aspect ratio $\Lambda = b/a$ and the OHNESORGE number. The OHNESORGE number is defined by

$$Oh = \sqrt{\frac{\rho\nu^2}{\sigma D_h}} = \frac{2}{Re_0} \text{ with } Re_0 = \frac{D_h v_0}{\nu}, \tag{3}$$

where ν denotes the kinematic viscosity. Note that the OHNESORGE number is inversely proportional to the REYNOLDS number based on the characteristic velocity from equation (1).

To obtain symmetric conditions at the free surface concerning the plane $y = 0$ and $z = 0$ the hydrostatic pressure caused by an acceleration $\mathbf{g} = (g_x, g_y, g_z)$ is required to be negligibly small compared to the capillary pressure. This holds for sufficiently small BOND numbers in all directions, given by

$$Bo_x = \frac{\rho g_x a l}{2\sigma} \ll 1, Bo_y = \frac{\rho g_y a^2}{2\sigma} \ll 1, Bo_z = \frac{\rho g_z a b}{2\sigma} \ll 1. \tag{4}$$

3 The Experimental Test Case

3.1 Experimental setup and procedure

The experimental setup and procedures are explained in detail in Rosendahl *et al.* (2003). Therefore just a brief overview is given below. The experiment was carried out under microgravity conditions on board the sounding rocket TEXUS-37. During the ballistic flight the rocket provides an all axis low gravity environment of $10^{-4} g_0$ (with g_0 the gravitational acceleration on earth) for six minutes. With the properties of the test liquid the maximum Bond number is $Bo = 5.6 \cdot 10^{-3}$ which satisfies the requirements of (4).

The schematic drawing of the experiment is shown in figure 2. Note that for the sake of clearness all technical details necessary for establishing the capillary channel flow under microgravity are omitted. The core element of the setup consists of a cylindrical liquid reservoir (no. 1) with a compensation tube (no. 2) and an observation chamber (no. 3) with the open channel. Via a nozzle (no. 4) the channel is connected to the liquid reservoir. The flow through the channel is established by two gear pumps. One pump supplies the reservoir with the volume flux Q_1 through a circular gap on the bottom of the reservoir covered by a screen. The second pump withdraws a volume flux Q_2 via the

Liquid properties	Characteristic numbers	Scaling values
$\rho = 766$ kg/m^3	$Oh = 0.00152$	$a/2 = 2.5$ mm
$\sigma = 15.8{\cdot}10^{-3}$ N/m	$\Lambda = 5.0$	$A_0 = 125$ mm^2
$\nu = 0.69{\cdot}10^{-6}$ m^2/s	$L = 18.66$	$v_0 = 90.8$ mm/s
$\gamma_s = 0°$		$p_0 = 6.32$ Pa

Table 1: Liquid properties for the test liquid DOW Corning SF 0.65 at $T = 20°$C, characteristic numbers and scaling values of the problem.

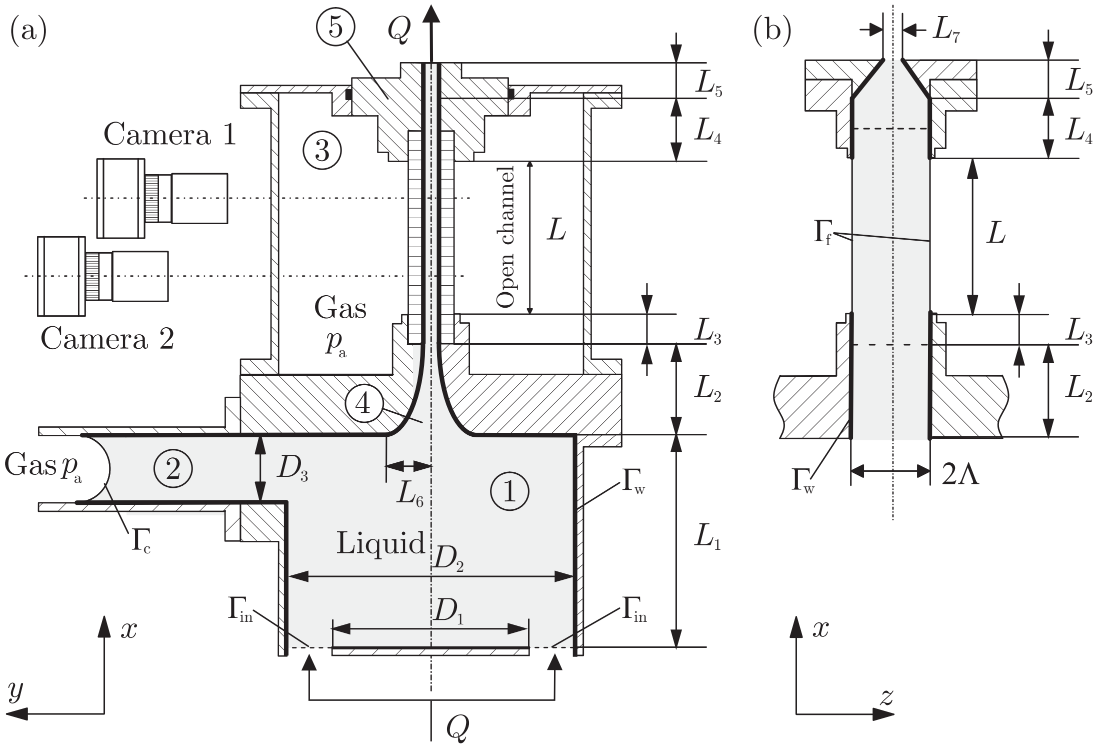

Figure 2: Schematic drawing of the experimental setup to investigate the open capillary channel flow on board the sounding rocket TEXUS-37. All technical details for establishing the flow under microgravity are omitted. The numbers denote: 1 liquid reservoir, 2 compensation tube, 3 observation chamber with the open channel, 4 nozzle, 5 outlet. All properties are dimensionless. (a) The (x, y) plane and (b) the (x, z) plane.

channel and the nozzle from the reservoir. The unavoidable difference of the volume fluxes between both pumps caused by fluctuations of the rotation speed and varying liquid slip inside the pump is compensated by the cylindrical compensation tube. For the numerical calculation the difference may be neglected yielding $Q_1 = Q_2 = Q$. With this assumption the position of the liquid meniscus inside the tube is fixed in the steady case. Since the used silicone oil (DOW Corning SF 0.65, liquid properties are given in table 1) is perfectly wetting the static contact angle on perspex and quartz glass is $\gamma_s = 0$. For this reason the liquid surface in the compensation tube of perspex always has the shape of a spherical calotte leading to a constant liquid pressure inside the tube. Note that liquid surfaces of the channel and of the compensation tube are exposed to the same ambient gas pressure p_a.

The capillary channel consists of two parallel quartz plates of (dimensionless) breadth 2Λ and distance 2. At the bottom end the plates are connected to the nozzle and to the outlet at the upper end (see figure 2). Both the nozzle and the outlet have a closed cross section so that the open section of the channel measures the length L. The nozzle was

Reservoir	Comp. tube	Nozzle	Open channel	Outlet
$D_1 = 26.0$	$D_3 = 18.0$	$L_2 = 12.0$	$\Lambda = 5$	$L_4 = 8.4$
$D_2 = 38.0$		$L_3 = 2.8$	$L = 18.66$	$L_5 = 4.8$
$L_1 = 30.0$		$L_6 = 6.0$		$L_7 = 3.6$

Table 2: Geometric values of the experimental setup. All length are scaled with $a/2 = 2.5$ mm.

designed to achieve quasi one-dimensional flow conditions at the inlet of the open channel section. It has a rectangular inlet cross section of $2L_6$ by 2Λ which constricts on the length L_2 to the channel cross section (2 by 2Λ). Note that all these dimensionless values are listed in table 2. In the (x, y)-plane the nozzle has an elliptical shape (see figure 2(a)) which corresponds to a quarter section of an ellipse between the principal axis $2L_2$ and $2(L_6 - 1)$. Downstream of the nozzle the channel cross section remains unchanged on the length L_3 before the flow enters the open section. With this form the lateral velocity components in the entrance cross section of the open channel were minimized to 2% of the longitudinal components. Concerning the longitudinal velocity distribution the flow is characterized by a constant core flow with small boundary layers at the sides. As shown in figure 2(b) the outlet cross section remains constant at first (length L_4), then it constricts on the length L_5 to a rectangular orifice of 2 by L_7. The reservoir is a cylindrical container with diameter D_2 and height L_1. The circular gap at the bottom is defined by the diameter D_1 and D_2. The compensation tube has a diameter of D_3.

The capillary channel was observed by two CCD cameras. On the front side of the upper plate precise markings for the calibration and evaluation of the video images are etched. As shown in figure 3(a) the views had an overlap around the middle markings (approximately 10 mm). Due to total reflection at the gas-liquid interfaces the liquid surfaces appear as dark zones on the video images. Referring to figure 3(c) these zones are the projection of the distance $\Lambda - k^L$ and $\Lambda - k^R$ into the image plane. The positions $k^L(x)$ and $k^R(x)$ correspond to the left and right hand side innermost contour lines of the surfaces, respectively.

During the experiment the volume flux Q was increased in small increments up to the critical value Q_{crit} at which the surfaces collapse and the ingestion of gas bubbles sets in. At any adjusted volume flux $Q < Q_{crit}$ yielding a steady flow both contour lines were detected by digital image processing and averaged in time. Finally for the comparison with the numerical calculations the mean innermost contour position $k = 0.5(k^L(x) - k^R(x))$ as function of Q is provided.

3.2 Test case parameter and boundary conditions

For the determination of the boundary condition at the channel inlet, it is necessary to compute the complete flow in the liquid reservoir and the nozzle. The pressure in the compensation tube is given by the curvature of its free surface. The flow in the outlet section has an effect and should be modeled too. The geometric data of the channel, the nozzle, the liquid reservoir, the compensation tube and the outlet are listed in table 2. Also the properties of the test liquid DOW Corning SF 0.65 are given in table 1.

The boundary conditions of the problem will be given in dimensionless form. In figure 2 all thick solid lines are walls Γ_{w} with no-slip condition:

$$\mathbf{u} = \mathbf{0} \text{ on } \Gamma_{\mathrm{w}}. \quad (5)$$

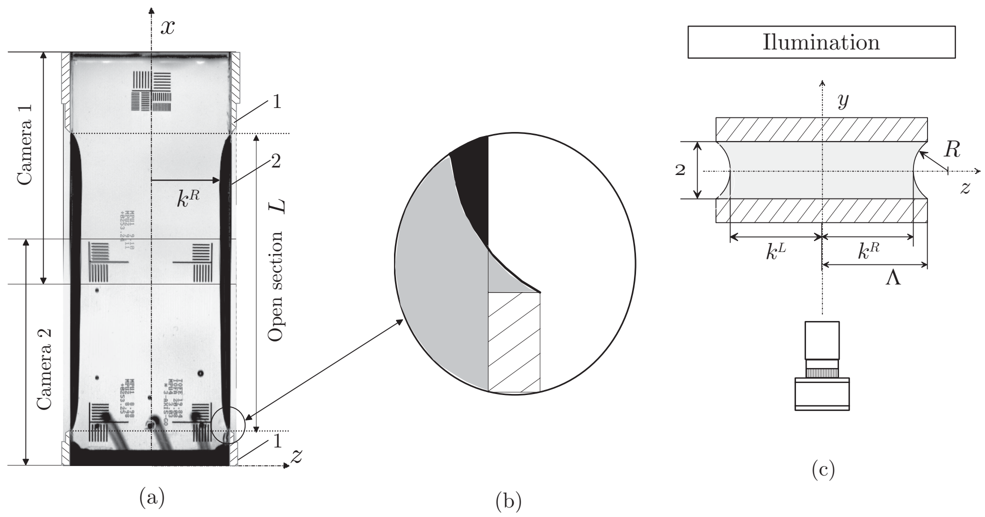

Figure 3: (a) Front view of the channel during the steady phase of the flow ($Q < Q_{crit}$). The optical axes of the cameras are aligned perpendicularly to the top plate. At the inlet and outlet the plates are covered by thin coated metal plates at the sides (1), which are depicted in detail in figure (b) (the fluid is drawing in gray). Due to total reflection the liquid surfaces (2) appear dark. The innermost surface positions correspond to the distances k^L and k^R in figure (c).

In case of steady flow, the liquid reservoir is supplied via the circular gap with the same volume flux Q, which is withdraw at the channel outlet. Because the inflow Γ_{in} has an area of $A_{\text{in}} = 30.16$, we obtain

$$\mathbf{u} = (u_{\text{x}}, 0, 0) \text{ on } \Gamma_{\text{in}} \text{ with } u_{\text{x}} = \frac{Q}{A_{\text{in}}} = \frac{Q}{30.16}, \tag{6}$$

whereby the volume flux is different for the different contour shapes and given in the results section. At the end of the free surface channel at $x = L$ we have

$$Q = \int_{-1}^{1} \int_{-\Lambda}^{\Lambda} u_{\text{x}} dz dx. \tag{7}$$

Additionally to these boundary conditions, the static pressure in the system is given by the capillary pressure at the free surface Γ_{c} of the compensation tube. The free surface is hemispherical with a static contact angle of $\gamma_s = 0°$. According to equation (2) with $R_1 = R_2 = 9$ we have

$$p - p_a = 0.2222 \text{ on } \Gamma_{\text{c}}. \tag{8}$$

No flow occurs in the compensation tube in the case of a steady flow.

The free surface in the open channel has the following conditions: If $\overline{z}(x, y)$ is the 3d free surface of our problem and $k(x) = \overline{z}(x, y = 0)$ the surface position in the symmetry plane $y = 0$ (see figure 3(c)) (note, that because of the symmetry with respect to the (x, y)-plane, we only give the values for $\overline{z}(x, y) \geq 0$), the boundary conditions for the free surface read

$$\begin{aligned} \overline{z}(x = 0, y) &= \Lambda_{\text{i}} \quad \text{and especially} \quad k(x = 0) = \Lambda_{\text{i}} \\ \overline{z}(x = l, y) &= \Lambda_{\text{o}} \quad \text{and especially} \quad k(x = l) = \Lambda_{\text{o}}. \end{aligned} \tag{9}$$

As shown in figure 3(b) the liquid wets the outer body of the inlet and outlet. To have a good coincidence between measured and calculated surface shapes $\Lambda_{\text{i}} = 5.076$ and

$\Lambda_\mathrm{o} = 5.11$ have to be applied to equation (9). For a first computational approach the choice of $\Lambda_\mathrm{i} = \Lambda_\mathrm{o} = \Lambda = 5.0$ is a good approximation. Note that the liquid surface is not necessarily pinned at the edges of the plates, so that $\overline{z}(x, y = \pm 1) < \Lambda$ for any positions $0 < x < L$. In case of unsteady flows the surface detaches form the edges and moves in between the plates (see section 4). The same effect may also occur for steady flows with large L. On the free surface Γ_f we have the kinematic and the dynamic boundary condition. The first one requires that the fluid velocity at the free boundary is equal to the velocity of the surface itself

$$\mathbf{u} \cdot \mathbf{n} = u_b \text{ on } \Gamma_\mathrm{f}, \tag{10}$$

where $\mathbf{n}$ is the unit outer normal vector and u_b is the normal velocity of the free surface. In the stress balance we neglect normal and tangential stresses and the pressure difference across the free surface is described by the Gauss-Laplace equation (2). Note that we have no surface tension variations. As initial condition for the unsteady case one can use a steady solution for $Q < Q_{crit}$ or a plane surface with $\mathbf{u} = \mathbf{0}$.

Summary of the required calculations

- The shape of the free surfaces in the symmetry plane $y = 0$ for different volume fluxes $Q < Q_{crit}$.
- The maximum volume flux Q_{crit}.
- The position of the smallest cross section and the maximum mean velocity for different volume fluxes $Q < Q_{crit}$.
- Qualitative behavior of the shapes of the free surface in the symmetry plane $y = 0$ for volume fluxes $Q > Q_{crit}$ at the times shown in figure 6.

4 Results

Figure 5 shows the flow for different volume fluxes with $Q < Q_{crit}$. Besides small harmonic oscillation of the free surface caused by the pumps the flow is steady. The surfaces are symmetrically with respect to the plane $z = 0$ and the mean contour line k is constant in time. With increasing volume flux the curvature of the liquid surface grows and the flow path constricts. At a certain volume flux the flow becomes unsteady as shown in figure 6, which is slightly above the critical value. The surface collapses and a periodic ingestion of gas bubbles is observed leading to a two phase flow suction-sided. During the bubble formation, which is symmetrical, the surface stayed pinned at the edge of the outlet. The experimental critical volume flux is $Q_{crit} = 0.738$ ($Q'_{crit} = 8.38$ ml/s).

Figure 4 shows the steady mean surface positions k (innermost contour line) along the channel axis x as a function of the adjusted volume flux Q. Due to insufficient contrast the contour points near the inlet and outlet could not be detected. For this reason the experimental contours in figure 4 and 7 do not meet the upper mentioned boundary condition. The labels refer to the evaluated sequences given in table 4. The labels indicate the chronological order in which the volume fluxes were adjusted during the experiment. The comparison of the sequences S-04 and S-07 (both at $Q = 0.689$), as well as S-05, S-06 and S-12 (all at $Q = 0.730$) shows that the flow conditions are reproducible. l^* denotes the length from the channel inlet at $x = 0$ up to the smallest cross section. This location of the flow path is of particular interest since the collapse of the liquid surface is initiated here. Each change of volume flux causes a pressure disturbance which travels upstream at a certain wave speed to change the inlet boundary condition. As shown by Rosendahl *et al.* (2003) the wave speed decreases with increasing curvature of the liquid surface.

	$Q_1' = 5.52$ ml/s $Q_1 = 0.486$	$Q_2' = 7.37$ ml/s $Q_2 = 0.649$	$Q_3' = 8.17$ ml/s $Q_3 = 0.718$	$Q_4' = 8.38$ ml/s $Q_4 = 0.738$
x	$k(x)$	$k(x)$	$k(x)$	$k(x)$
0.3732	5.0188	4.9318	4.9042	4.8987
0.7464	4.8971	4.8254	4.7879	4.7789
1.1196	4.8393	4.7566	4.7100	4.6984
1.4928	4.8136	4.7185	4.6642	4.6511
1.8660	4.7932	4.6915	4.6310	4.6169
2.2392	4.7829	4.6743	4.6092	4.5937
2.6124	4.7751	4.6622	4.5927	4.5754
2.9856	4.7711	4.6537	4.5817	4.5627
3.3588	4.7671	4.6473	4.5720	4.5536
3.7320	4.7645	4.6431	4.5660	4.5459
4.1052	4.7620	4.6380	4.5590	4.5361
4.4784	4.7604	4.6344	4.5530	4.5323
4.8516	4.7581	4.6308	4.5488	4.5258
5.2248	4.7561	4.6278	4.5436	4.5197
5.5980	4.7542	4.6245	4.5380	4.5142
5.9712	4.7528	4.6209	4.5325	4.5078
6.3444	4.7508	4.6175	4.5278	4.5020
6.7176	4.7492	4.6141	4.5229	4.4962
7.0908	4.7471	4.6104	4.5174	4.4895
7.4640	4.7452	4.6067	4.5127	4.4844
7.8372	4.7425	4.6030	4.5063	4.4787
8.2104	4.7410	4.5982	4.5007	4.4696
8.5836	4.7381	4.5954	4.4954	4.4643
8.9568	4.7359	4.5915	4.4898	4.4577
9.3300	4.7347	4.5876	4.4832	4.4500
9.7032	4.7341	4.5859	4.4787	4.4442
10.0764	4.7322	4.5828	4.4746	4.4388
10.4496	4.7297	4.5785	4.4689	4.4323
10.8228	4.7269	4.5741	4.4624	4.4252
11.1960	4.7239	4.5709	4.4554	4.4171
11.5692	4.7218	4.5655	4.4485	4.4071
11.9424	4.7196	4.5608	4.4411	4.3975
12.3156	4.7178	4.5560	4.4322	4.3853
12.6888	4.7132	4.5496	4.4228	4.3763
13.0620	4.7113	4.5466	4.4170	4.3674
13.4352	4.7102	4.5440	4.4108	4.3591
13.8084	4.7082	4.5396	4.4051	4.3522
14.1816	4.7068	4.5365	4.4000	4.3456
14.5548	4.7054	4.5343	4.3953	4.3390
14.9280	4.7050	4.5324	4.3922	4.3360
15.3012	4.7045	4.5312	4.3925	4.3362
15.6744	4.7047	4.5331	4.3962	4.3399
16.0476	4.7080	4.5383	4.4045	4.3518
16.4208	4.7125	4.5473	4.4207	4.3698
16.7940	4.7246	4.5650	4.4476	4.4029
17.1672	4.7462	4.5979	4.4920	4.4524
17.5404	4.7858	4.6514	4.5593	4.5231
17.9136	4.8546	4.7386	4.6695	4.6434
18.2868	4.9952	4.9056	4.8374	4.8170

Table 3: Evaluated mean surface position k from the experiment in dependence of the flow path x. Q_1 is the lowest and Q_4 is the highest volume flux of the steady flow.

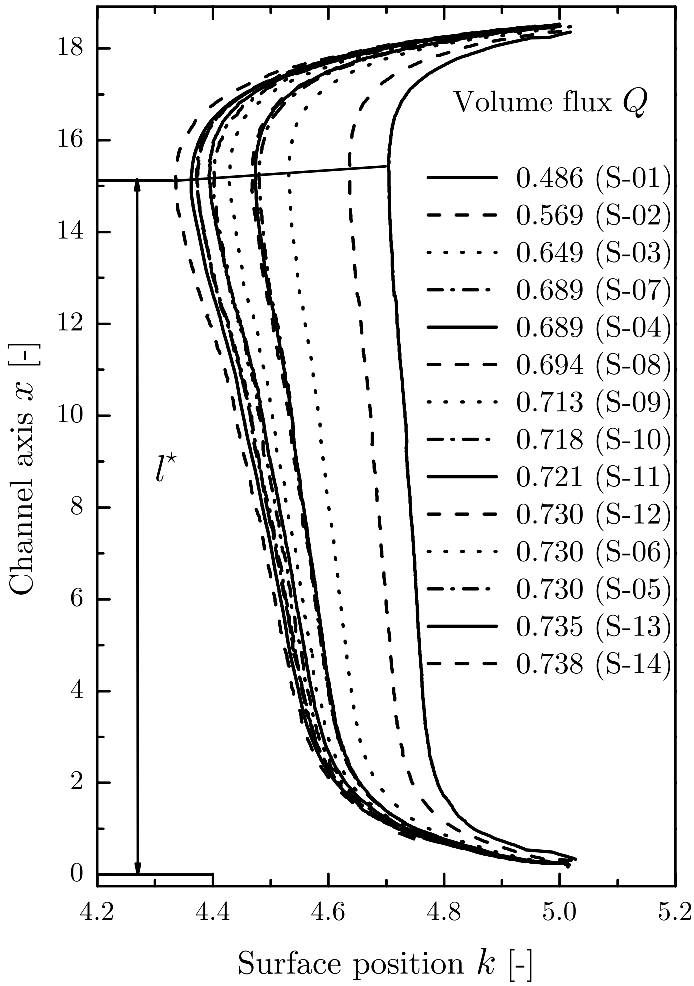

Figure 4: Experimental determined mean surface position $k(x)$ as function of the volume flux Q for the TEXUS-experiment.

For this reason an increase of the volume flux increases the liquid velocity but decreases the wave speed so that the speed of the pressure disturbance relative to the liquid flow vanishes for the critical volume flux Q_{crit} at the smallest cross section. Since the upstream boundary condition remains unchanged at that state gas is ingested into the outlet for the sake of mass conservation. Table 4 provides the mean surface position k^* and the mean liquid velocity v^* at the smallest cross section $x = l^*$ at steady flow conditions. In figure 7 four experimental contour lines of the steady flow are exemplified in detail. The error of the contour evaluation is $\Delta k = \pm\ 0.036$. All contour data are given in table 3.

5 Acknowledgement

The funding of the sounding rocket flight by the European Space Agency (ESA) and the funding of the research project by the Ministry of Education and Research (BMBF) and the German Aerospace Center (DLR) under grant numbers 50WM0241 and 50WM9901 are gratefully acknowledged.

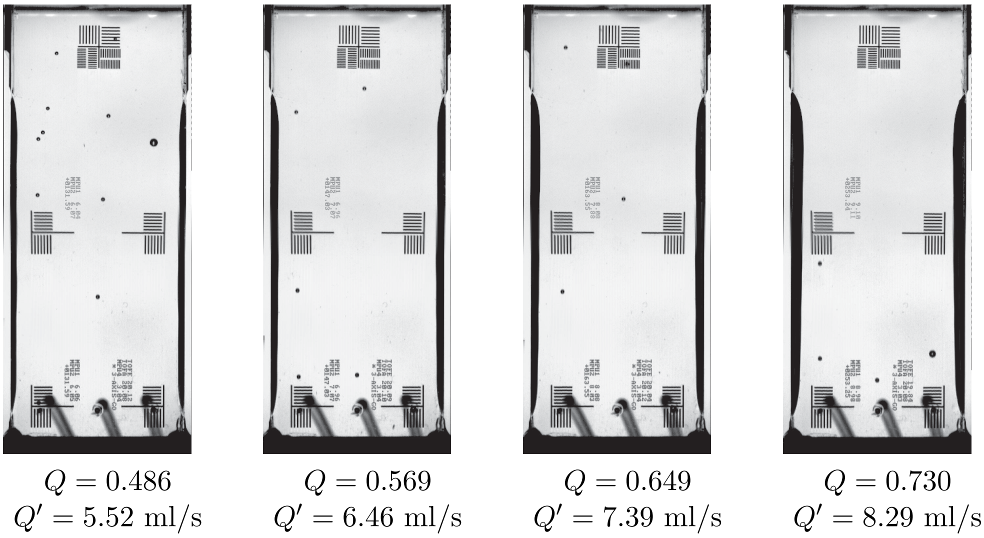

Figure 5: Steady liquid flow in the open capillary channel at different volume fluxes below the critical value, $Q < Q_{\rm crit}$. The flow direction is from the bottom to the top. Due to the increasing pressure loss the flow path narrows with increasing volume flux.

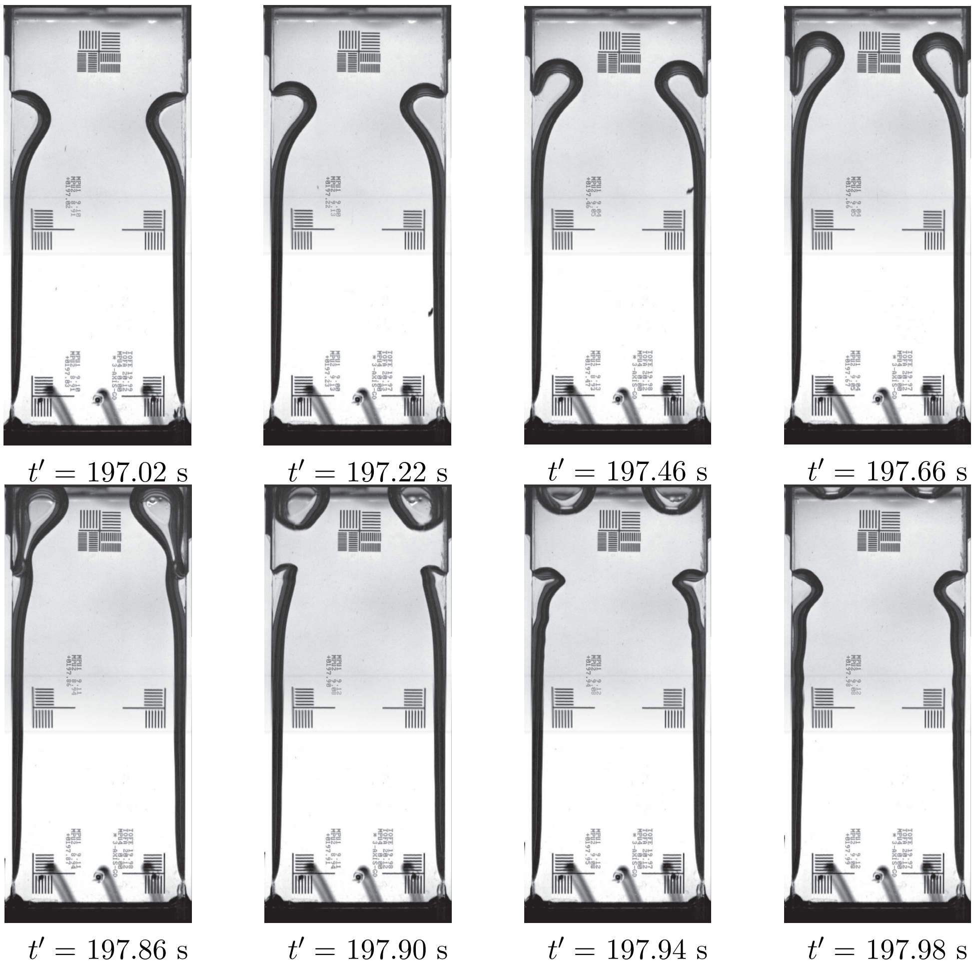

Figure 6: Typically unsteady liquid flow in the open capillary channel at a fixed volume flux above the critical value, $Q > Q_{crit}$. The free surfaces collapse and a periodic ingestion of gas bubbles is observed. The bubble formation occurs symmetrically as shown here.

No.	Q' [ml/s]	Q [-]	k'^* [mm]	k^* [-]	l'^* [mm]	l^* [-]	v'^* [mm/s]	v^* [-]
S-01	5.52	0.486	11.76 ± 0.09	4.704± 0.036	38.48 ± 0.25	15.39±0.1	46.0 ± 2.5	0.506±0.028
S-02	6.46	0.569	11.59 ± 0.09	4.636±0.036	38.82 ± 0.25	15.53±0.1	54.4 ± 3.0	0.598±0.033
S-03	7.39	0.649	11.33 ± 0.09	4.532±0.036	38.04 ± 0.25	15.22±0.1	63.1 ± 3.5	0.694±0.039
S-04	7.82	0.689	11.18 ± 0.09	4.472±0.036	38.03 ± 0.25	15.21±0.1	67.7 ± 3.8	0.745±0.042
S-05	8.29	0.730	10.93 ± 0.09	4.372±0.036	37.54 ± 0.25	15.02±0.1	72.9 ± 4.1	0.802±0.045
S-06	8.29	0.730	10.93 ± 0.09	4.372±0.036	37.54 ± 0.25	15.02±0.1	72.9 ± 4.1	0.802±0.045
S-07	7.82	0.689	11.20 ± 0.09	4.480±0.036	38.03 ± 0.25	15.21±0.1	67.5 ± 3.8	0.743±0.042
S-08	7.87	0.694	11.17 ± 0.09	4.468±0.036	37.20 ± 0.25	14.88±0.1	68.1 ± 3.8	0.750±0.042
S-09	8.10	0.713	11.07 ± 0.09	4.428±0.036	37.64 ± 0.25	15.06±0.1	70.5 ± 4.0	0.776±0.044
S-10	8.15	0.718	11.00 ± 0.09	4.400±0.036	37.59 ± 0.25	15.04±0.1	71.3 ± 4.0	0.785±0.044
S-11	8.19	0.721	10.98 ± 0.09	4.392±0.036	38.03 ± 0.25	15.21±0.1	71.7 ± 4.0	0.789±0.044
S-12	8.29	0.730	10.93 ± 0.09	4.372±0.036	37.69 ± 0.25	15.08±0.1	72.9 ± 4.1	0.802±0.045
S-13	8.34	0.735	10.92 ± 0.09	4.368±0.036	37.49 ± 0.25	15.00±0.1	73.4 ± 4.1	0.808±0.045
S-14	8.38	0.738	10.87 ± 0.09	4.348±0.036	37.74 ± 0.25	15.10±0.1	74.0 ± 4.2	0.815±0.046

Table 4: Evaluated data from the experiment on board of TEXUS-37 in temporal order: volume flux Q, mean surface position k^* and mean fluid velocity v^* at the smallest cross section $x = l^*$.

References

Dreyer, M. E., Delgado, A., & Rath, H. J. 1994. Capillary Rise of Liquid Between Parallel Plates under Microgravity. *J. Colloid Interface Sci.*, **163**, 158–168.

Jaekle, Jr., D. E. 1991. Propellant Management Device Conceptual Design and Analysis: Vanes. AIAA Paper, nos. 91–2172.

Landau, L. D., & Lifschitz, E. M. 1991. *Lehrbuch der Theoretischen Physik, Band VI, Hydrodynamik*. Berlin: Akademie Verlag.

Rosendahl, U., Ohlhoff, A., Dreyer, M. E., & Rath, H. J. 2002. Investigation of Forced Liquid Flows in Open Capillary Channels. *Microgravity Sci. Technol.*, **XIII/4**, 53–59.

Rosendahl, U., Ohlhoff, A., & Dreyer, M. E. 2003. Choked flows in open capillary channels: theory, experiment and computations. *J. Fluid Mech.* submitted.

Srinivasan, R. 2003. Estimating zero-g flow rates in open channels having capillary pumped vanes. *Int. J. Numer. Meth. Fluids*, **41**, 389–417.

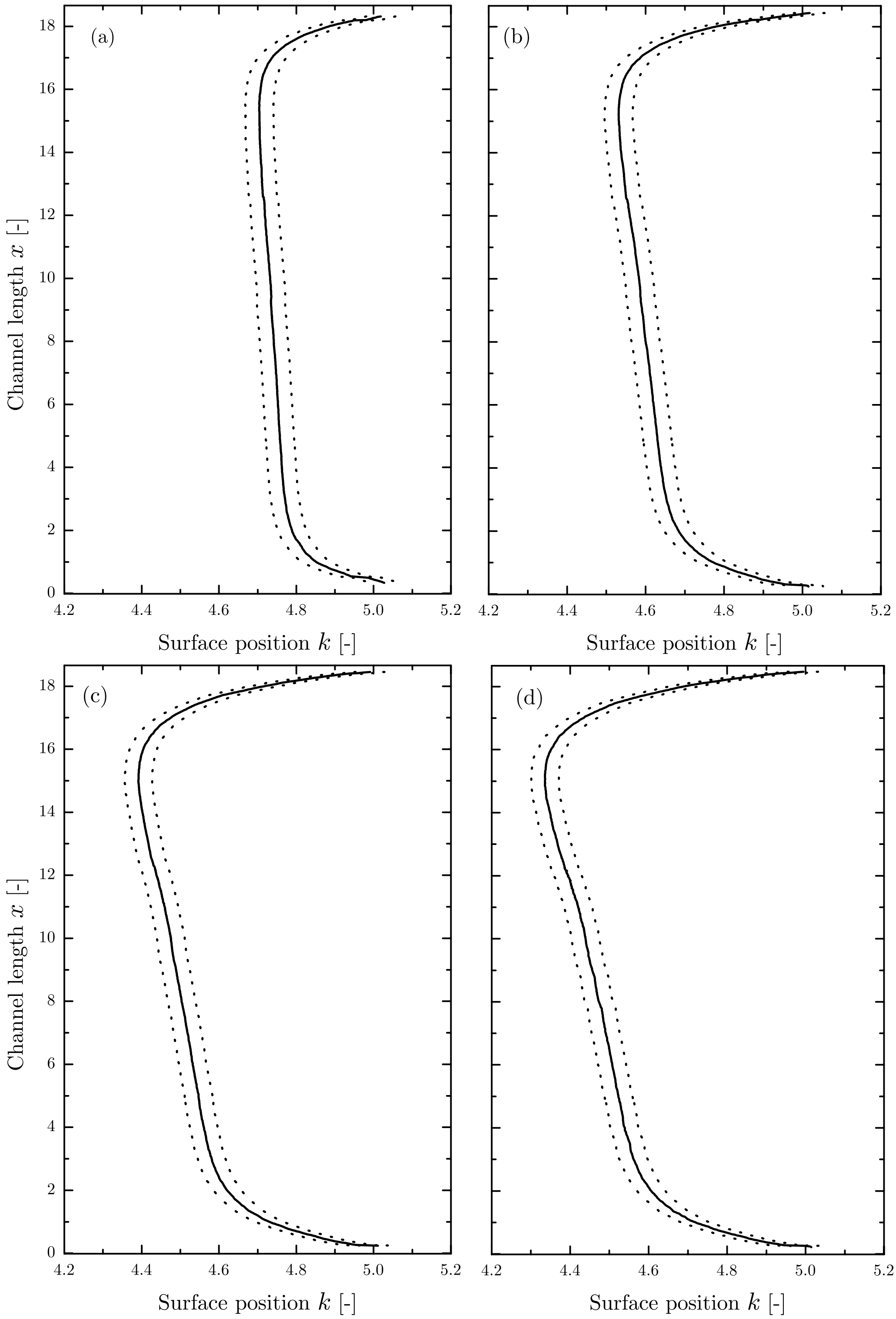

Figure 7: Evaluated mean surface position $k(x)$ from the experiment (solid lines) at different steady volume fluxes: (a) $Q = 0.486$ (S-01), (b) $Q = 0.649$ (S-03), (c) $Q = 0.718$ (S-10), (d) $Q = 0.738$ (S-14). The error of the contour data is displayed by dotted lines.